Environmental Nanotechnology, Monitoring & Management 20 (2023) 100805

Contents lists available at ScienceDirect

Environmental Nanotechnology, Monitoring & Management

journal homepage: www.elsevier.com/locate/enmm

Highly adsorptive removal of palladium and platinum ions from wastewater using novel ethylenediamine-glutaraldehyde-grafted metal organic framework

Thabiso C. Maponya [a,*], Katlego Makgopa [b], Thabang R. Somo [a], David M Tshwane [c], Kwena D. Modibane [a,*]

[a] Nanotechnology Research Lab, Department of Chemistry, School of Physical and Mineral Sciences, University of Limpopo (Turfloop), Sovenga 0727, Polokwane, South Africa
[b] Department of Chemistry, Faculty of Science, Tshwane University of Technology (Arcadia Campus), Pretoria 0001, South Africa
[c] Advanced Materials Engineering, Materials Science and Manufacturing, Council for Scientific and Industrial Research, PO Box 395, Pretoria 0001, South Africa

ARTICLE INFO

Keywords:
Adsorption
Metal–organic framework
Palladium
Platinum
Post-synthetic functionalization
Wastewater treatment

ABSTRACT

Herein, a metal–organic framework (MIL-101(Cr)) was synthesized and functionalized with ethylenediamine-glutaraldehyde (ED-GA for removal of palladium (Pd^{2+}) and platinum (Pt^{4+}) from wastewater. The chemical structure, surface properties, morphology, and adsorption energy of the prepared materials, MIL-101(Cr) and MIL-101(Cr)/ED-GA were analyzed using several analytical techniques and density functional theory (DFT). The prepared MIL-101(Cr)/ED-GA was efficient in removing Pd^{2+} and Pt^{4+} from aqueous solution with the percentage removal reaching 95% for Pd^{2+} and 85% for Pt^{4+}. Furthermore, the adsorption data demonstrated a good fit to the Langmuir isotherm model and gave the maximum adsorption capacity values of 416.17 mg g^{-1} for Pt^{4+} and and 322.6 mg g^{-1} for Pd^{2+} ions. Kinetics data obeyed a pseudo-second-order model and revealed the rapid adsorption of Pd^{2+} and Pt^{4+} ions by MIL-101(Cr)/ED-GA which reached equilibrium within 10 and 40 min, respectively. Lastly, DFT studies revealed that the adsorption of Pd^{2+} ions by the composite forms a more thermodynamically stable compound than adsorption of Pt^{4+}, suggesting that the material easily interacts with Pd and high selectivity is thus expected. This was indeed confirmed by experimental selectivity test results. Owing to their high affinity for PGMs, N atoms depicted large adsorption energy values compared to other adsorption sites. The MIL-101(Cr)/ED-GA could act as an efficient and cost effective adsorbent for removal of platinum group metals from wastewater.

1. Introduction

Palladium (Pd) and platinum (Pt) are the widely used luxurious members of the platinum group metals (PGMs) due to their exceptional behavior in catalysis. Consequently, their consumption increases owing to the advancing global economy and technology (Wasikiewicz et al., 2007). In order to meet the intensifying demand, more research is driven towards the recovery and recycling of Pd and Pt from secondary sources such as spent adsorbent, electronic scraps and mining tailings (Nikoloski et al., 2015). These efforts are aimed at reducing resource wastage and adverse environmental impacts. Over the years, different technologies such as liquid–liquid extraction (Zhang et al., 2020), cloud point extraction (Yuanpei et al., 2012), chemical precipitation (Yousif, 2019), membrane separation (Fajar et al., 2021), and adsorption (Maponya et al., 2020) have been successfully employed in the recovery and separation of these PGMs from wastewater to some extent. However, most of these methods have some drawbacks including generation of secondary contamination, poor removal efficacy, high operational expenses and complexity (Göksungur et al., 2005). Amongst the explored techniques, adsorption technology has emerged as a better method employed in the removal of metal ion complexes owing to its simple operation, low secondary pollution, and low cost (Arora, 2019); (Dabrowski, 2001). The adsorption method needs effective adsorbents such as resins (Fujiwara et al., 2007), magnetic nanomaterials (Uheida et al., 2006), activated carbon (Snyders et al., 2014), polymer fibers (Fayemi et al., 2013), and metal–organic framework (MOF) materials (Lin et al.,

* Corresponding authors.
E-mail addresses: thabiso.maponya@ul.ac.za (T.C. Maponya), Kwena.modibane@ul.ac.za (K.D. Modibane).

https://doi.org/10.1016/j.enmm.2023.100805
Received 1 October 2022; Received in revised form 19 January 2023; Accepted 1 March 2023
Available online 5 March 2023

2019).

MOFs are coordinated polymers, which are made of organic linkers and metal ions through coordination bond. Their unique and outstanding characteristics include easily tunable structures, adjustable porosity, as well as large specific surface areas (Makhafola et al., 2021). This encouraged their widespread development and applications, including hydrogen storage (Monama et al., 2019), gas sensing (Mashao et al., 2019) and capturing (Mabokela et al., 2022), drug delivery (Sun et al., 2020), electrochemical energy storage (Teffu et al., 2022), wastewater treatment (Tang et al., 2022), and other fields. In the case of Pd and Pt adsorption, MOFs including Matérial Institut Lavoisier (MIL)-101, MOF-802, Universitetet i Oslo (UiO)-66 and MOF-808 have managed to resolve some of the current water pollution crisis. For instance, Lin *et al.* (Lin et al., 2019) studied the Pd adsorptive capabilities of MOF-802, UiO-66, and MOF-808 at ambient temperature. The authors reported that maximum adsorption capacity of MOF-808, UiO-66 and MOF-802 for Pd^{2+} were 164, 105 and 26 mg g^{-1}, respectively. In a different study, Lin and co-workers (Lin et al., 2019) studied the binding ability of Pt^{4+} on the surface of UiO-66 in an acidic medium. After contacting 0.01 g of UiO-66 with 100 mg L^{-1} of Pt^{4+} solution at a pH of 1.0 for a day, they achieved the maximum adsorption capacity of 144 mg g^{-1}. Apart from these types of MOFs, MIL-101(Cr)-type MOFs possess some exceptional properties and are known to be chemically and thermally stable because of the strong Cr-O bonding between metal ions and organic ligands (Leng et al., 2016); (Burrows et al., 2012). MIL-101 (Cr) consists of Cr nodes $[Cr_3(OH)(H_2O)_2O(–CO_2)_6]$ and 1,4-dicarboxylic acid-type (H_2BDC or BDC) ligands. Another advantage of using MIL-101(Cr) is that the BDC organic linker can be easily prepared from polyethylene terephthalate (PET) waste bottles (Ren et al., 2016). The successful usage of PET to synthesize MOFs offers an economically favourable approach for waste management. However, it has been shown that the unmodified MOF material has certain limitations when used in adsorption, including unstable structure, low adsorption capacity, and poor selectivity (Luo et al., 2016).

Therefore, the versatile groups are usually incorporated by post-synthetic functionalization onto the organic ligand or metal cluster (Wang et al., 2017). Luo *et al.* (Luo et al., 2015) post-modified MIL-101 (Cr) with ethylenediamine (ED) through a benzene ring of organic linker site for the adsorptive removal of toxic divalent lead (Pb^{2+}) from aqueous solution. The amino functional groups increased the adsorption capacity from 15.7 to 87.64 mg g^{-1}. In the recovery of PGMs, Lim *et al.* (Lim et al., 2020) used amine-functionalized MIL-101(Cr) which was post-synthesized from amino and nitro-functionalized MIL-101(Cr) on the organic linker and tested in the uptake of Pd^{2+} and Pt^{4+} ioms from acidic aqueous solutions. They observed that MIL-101(Cr)–NH_2 performs much better and possessed higher adsorption capacities for both Pd^{2+} and Pt^{4+} than MIL-101(Cr)–NO_2. However, the observed capacity was still low for recovery of PGMs in real life application. The post-synthetic functionalization of MIL-101(Cr) with glutaraldehyde (GA) was reported by Ragheb *et al.* (Ragheb et al., 2022). The GA has often been used as a crosslink or grafting technology due to its ease in fabrication and effectiveness. Chemical modification of MIL-101(Cr) with GA changes its morphology and structure, which in turn affects the adsorption properties (Luo et al., 2016). Therefore, the combination of ED and GA as low molecular weight molecules with a relatively small kinetic diameter containing the amino and carbonyl groups have the potential to interact with Pd^{2+} and Pt^{4+} ions. Their interaction occurs between the aldehyde groups of GA and amine groups of ED on the MIL-101(Cr) surface. This results in the formation of an extra amide group to provide further active sites to interact with Pd and Pt metal ions. Hence herein, MIL-101(Cr) was synthesized from a PET waste bottle using the hydrothermal method. The introduction of ED on the Cr node was prepared by post-synthetic functionalization of MIL-101(Cr) followed by further grafting with GA for additional functional groups. Then the obtained MIL-101(Cr)/ED-GA adsorbent was used for the first time to adsorb Pd^{2+} and Pt^{4+} ions from aqueous environment. The adsorption behavior and capacity of MIL-101(Cr)/ED-GA was investigated under different factor conditions. Together, the adsorption isotherms and kinetics were studied, followed by the investigation of the potential reusability of the adsorbent.

2. Materials and methods

2.1. Reagents and chemicals

Chromium nitrate nanohydrate $Cr(NO_3)_3{\cdot}9H_2O$, Sigma-Aldrich, 99.5%), ethylene glycol ($HOCH_2CH_2OH$, Sigma-Aldrich, 99.8%), sodium hydroxide (NaOH, Sigma-Aldrich, 99.8%), hydrochloric acid (HCl, Sigma-Aldrich, 99.8%), ethylenediamine ($C_2H_8N_2$, Sigma-Aldrich, 99.8%) and glutaraldehyde ($C_5H_8O_2$, Sigma-Aldrich, 99.8%) were used as received. PET bottles were collected from the University of Limpopo dining Hall, Polokwane, South Africa. Upon removing caps, rings, and labels, the bottles were cut and shaped into smaller chips.

2.2. Synthesis of MIL-101(Cr)/ED-GA

The synthetic procedures were conducted in a 100 mL Teflon-lined hydrothermal reactor (Laboratory Supplies, South Africa) (Ren et al., 2016). BDC was prepared from a PET waste bottle (Scheme 1). Briefly, 3.00 g of PET flakes and 6.00 mL ethylene glycol (EG) were placed into the reactor together with 60.00 mL H_2O. The reaction vessel was heated and kept at 210 °C for 8 h. The resultant white particles were separated by centrifuge, prior to washing with ethanol, then followed by drying at 100 °C over night in an oven.

Chromium-based MIL-101 as shown in Scheme 1, was synthesized based on the reported procedure (Shafiei et al., 2018). Approximately, 4.00 g of $Cr(NO_3)_3{\cdot}9H_2O$ salt and 1.66 g of H_2BDC were suspended in deionized H_2O. and subsequently stirred for 15 min prior to ultra-sonic mixing for 0.5 h. The reaction mixture was put into an autocleavable reactor and kept in an oven for 8 h at 220 °C. The resulting product (MIL-101(Cr)) was filtered, washed and dried under 100 °C.

The grafting with ED as indicated in Scheme 1was done under refluxing by dispersing 0.50 g of the prepared MIL-101(Cr) in anhydrous toluene (50.00 mL), then added ED (1.00 mL). After 12 h, the obtained brown ED@MIL-101(Cr) precipitates were separated by vacuum filtration, followed by washing with ethanol and finally allowed to dry at 60 °C over night.

Preparation of the glutaraldehyde grafted ED@MIL-101(Cr) (Scheme 1) was perfomed by suspending 0.50 g of ED@MIL-101(Cr) in 50.00 mL of glutaraldehyde solution. The reaction suspension was kept under stirring for 24 h at 25 °C. Then, MIL-101(Cr)/ED-GA particulates were separated by vacuum filtration and dried at 60 °C for overnight.

2.3. Characterizations

Structural studies of MIL-101(Cr)/ED-GA with reference to MIL-101 (Cr) were deduced from X-ray diffraction Phillips 1830 instrument with a wavelength (λ) peak positioned at 1.54 Ã…. Functional groups elucidation and Fourier transform infrared (FT-IR) spectroscopic studies were explored from the Agilent Cary 600 Series, Spectrum II PerkinElmer. The Brunauer-Emmett-Teller (BET) isothermal curves were analysed using Micromeritics Tristar 300, where the samples were first degassed at 180 °C for 4 h prior to nitrogen gas adsorption–desorption. Perkin-Elmer STA 6000 instrument was used to study the thermal properties of the samples under N_2 gas ejected at 20 mL min^{-1}. The surface morphology, elemental analysis, and mapping were probed by using FE-SEM (Auriga Cobra focused-ion beam scaning electron microscopy fitted with energy dispersive X-ray (EDS), operated at 200 keV.

2.4. Sorption experiments

The pH studies were investigated from 1.00 to 6.00 for Pd^{2+} and

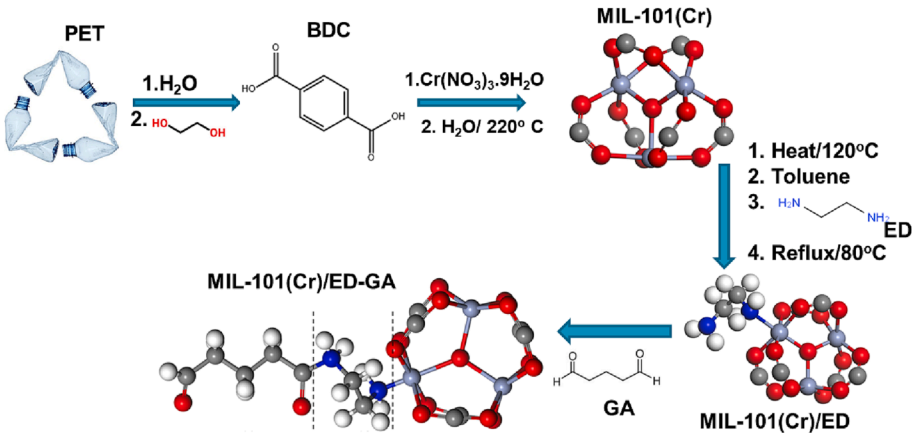

Scheme 1. Preparation of MIL-101/ED-GA from waste PET bottle.

Pt^{4+}at 100 mg L^{-1} and 50.0 mL volume using HCl and NaOH for adjustments. The effects of initial concentrations on Pd^{2+} and Pt^{4+} sorption by MIL-101(Cr)/ED-GA were explored from 50 to 400 mg L^{-1} at 25 °C.. Kinetics experiments were assessed with an optimum adsorbent amount and pH, of 0.03 g and pH of 3.0 for Pd^{2+}; and 0.02 g and pH of 4.0 for Pt^{4+}. The remaining concentrations of Pd^{2+} and Pt^{4+}, before and after adsorption were determined from the ultraviolet–visible (UV–Vis) spectroscopy (Lambda 365 UV/Vis Spectrophotometer, (PerkinElmer, Johannesburg, South Africa)). The removal efficiency of the composites was deduced from Equation (1):

$$\%removal = \left(\frac{C_0 - C_e}{C_0}\right) X100 \quad (1)$$

C_o and C_e (mg L^{-1}) are the original and equilibrium concentrations of metal ions. The adsorption equilibrium adsorption capacity was estimated using the following equation:

$$q_e = \left(\frac{C_0 - C_e}{m}\right) V \quad (2)$$

where q_e (mg g^{-1}) is the quantity of metal ion adsorbed per unit mass of MIL-101(Cr)/ED-GA at equilibrium. m (g) and V (L) denote the amount of MIL-101(Cr)/ED-GA, and the volume of metal ion solution. Regeneration and reusability of the MIL-101(Cr)/ED-GA adsorbent were investigated by stirring the prepared adsorbent in a solution containing 6 M HCl solution after the adsorption. This was followed by thorough washing with deionized water prior to the subsequent cycle.

2.5. Simulation setup

All density functional theory (DFT) calculations were carried out using the $Dmol^3$ code module of the Material Studio software. The geometry optimization was computed using the exchange-correction functional of the Perdew-Berke-Ernzerhof (PBE) functional. Localized electron double numerical basis sets with polarization functions were used to enhance a set of numerical atomic orbitals. The structural optimization and energy calculation parameters' convergence conditions of maximum energy and force tolerance of 1.0105 Ha and 2.010 Ha/Å, respectively. A maximum displacement tolerance was set to 5.0103 Å. In order to determine the adsorption stability of palladium (Pd) and platinum (Pt) on MIL-101(cr)/ED-GA, adsorption energies were computed as given in Equation (3):

$$E_{ads.} = E_{MIL-101(Cr)/ED-GA/molecule} - \left(E_{MIL-101(Cr)/ED-GA} + \frac{1}{2}E_{molecule.}\right) \quad (3)$$

Where, $E_{MIL-101(Cr)/ED-GA/molecule}$, $E_{MIL-101(Cr)/ED-GA}$ and $\frac{1}{2}E_{molecule}$ are the total energies of MIL-101(Cr)/ED-GA/molecule, MIL-101(Cr)/ED-GA and molecules (palladium and platinum) structures. Fig. 1 depicts the atomic structure of MIL-101(Cr)/ED-GA with the binding energy of −8.820 Ha.

3. Results and discussions

3.1. Structural characterizations

Fig. 2(a) represent the FT-IR spectra for MIL-101(Cr) and MIL-101 (Cr)/ED-GA. The IR spectra demonstrated characteristic bands assigned to the benzene-carboxylates vibrations at 1510 and 1414 cm^{-1} for C = O and C-O bonding in the carboxylates (Abroudi et al., 2022). The band at 1631 cm^{-1} is due to the C = C of the benzene ring and the observed peak at 674 cm^{-1} is associated with Cr-O vibration (Zhuo et al., 2017). With the addition of ethylenediamine-glutaraldehyde, the peak intensities of C = O at around 1510 cm^{-1} decreased. The characteristic bands attributed to the amine and amide group in MIL-101(Cr)/ED-GA were seen at 3221 cm^{-1} for N-H stretch, 2944 cm^{-1}, and 1357 cm^{-1} for C-H and C-C stretching of the aliphatic CH_2 group, 1554 cm^{-1} for N-H bend and 1052 cm^{-1} for C-N stretch of the amide group in ethylenediamine-glutaraldehyde (Abroudi et al., 2022); (Modrow et al., 2012); (Jalayeri et al., 2020). In addition, a new peak appeared at 506 cm^{-1} which is assigned to the N-Cr vibrations indicating the successful preparation of MIL-101(Cr)/ED-GA.

Fig. 2(b) shows the XRD patterns of the prepared MOF samples obtained in the range of 5–80 2θ degrees. The diffraction pattern for MIL-101(Cr) revealed characteristic peaks at 5.59°, 8.63°, 9.25°, 9.90°, 10.6°, 11.7°, 16.8°, 17.6°, 18.2°, and 19.2° which correspond with the reported studies (Zhuo et al., 2017); (Vo et al., 2020); (Anılır et al., 2020). In comparison to the MIL-101(Cr)/ED-GA patterns, it was seen that post-synthetic functionalization has some effect on the symmetry of

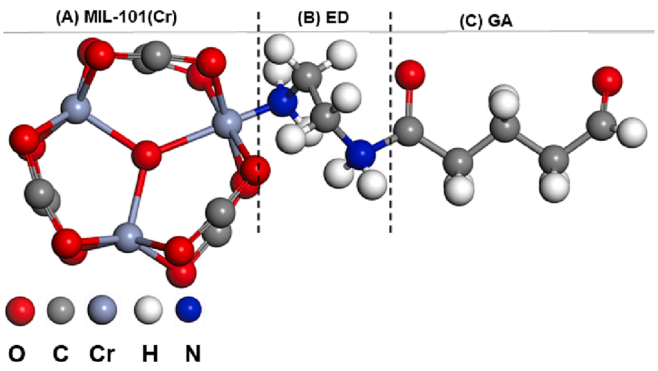

Fig. 1. Present the atomic structure of MIL-101(Cr)/ED-GA.

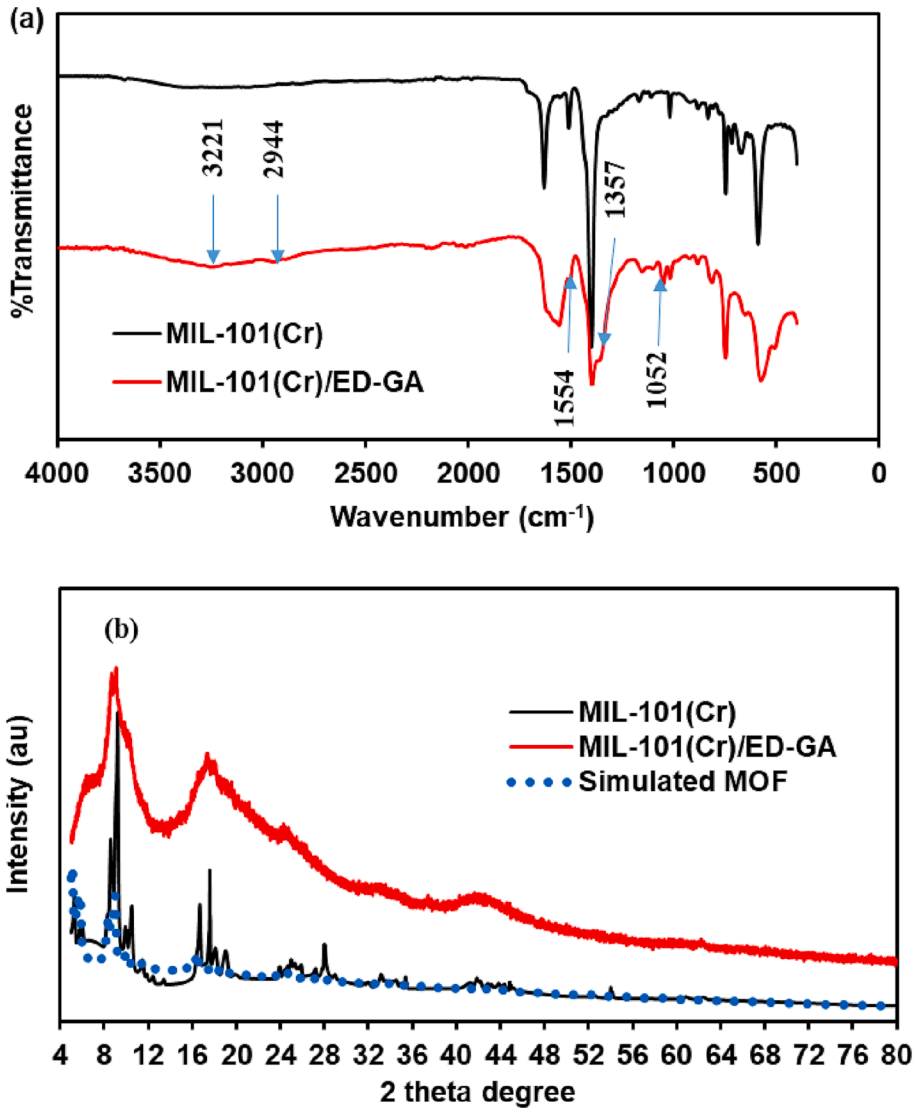

Fig. 2. (a) FTIR and (b) Diffractograms for MIL-101(Cr) and MIL-101(Cr)/ED-GA.

the crystal as the diffraction peaks broadened. However, the framework of the MIL-101(Cr) was not destroyed as the major characteristic peaks were still observed on the MIL-101(Cr)/ED-GA patterns. This was further supported by determining the amount of MIL-101(Cr) crystallinity in the MIL-101(Cr)/ED-GA using Vegard's law (Jacob et al., 2007). The calculated value for the lattice period parameters (a = b = c) was 68.0 Å and gave 75.1% crystallinity. The reduced crystallite size in MIL-101(Cr)/ED-GA was also calculated at 2θ degrees using the Debye-Scherrer formula (Somo et al., 2021) shown by Equation (4) and found to be 6.1 nm.

$$D = \frac{0.9\lambda}{\beta \mathrm{Cos}\theta} \tag{4}$$

The BET analyses of MIL-101 and MIL-101(Cr)/ED-GA are depicted by Fig. 3(a)-(c). As illustrated in Fig. 3(a,b), MIL-101(Cr) and MIL-101 (Cr)/ED-GA possessed type I isotherm curves, which suggest the presence of microporous structure of the adsorbents. The steep slope is resulting from the slow adsorption of N_2 by the smaller microporous cavities of MIL-101(Cr) (Hasan et al., 2013); (Hu et al., 2017). The initial steep slope is then followed by a narrow hysteresis loop in pressures between $0.25 < P/P_0 < 0.95$, signifying mesopores with uniform pore size distribution. Oppositely, Fig. 2(b) shows that N_2 struggles to penetrate the pores of MIL-101(Cr)/ED-GA at lower P/P_0 values. This can suggest that the material is dominated by very small pores and thus the diffusion is very slow. In both cases, however, an abrupt increase in the N_2 amount is noted when P/P_0 is higher than 0.9. In addition, the surface area of MIL-101(Cr) was measured as 308.73 $m^2\ g^{-1}$ with a pore volume of 0.122 $cm^3\ g^{-1}$. For MIL-101(Cr)/ED-GA, the values decreased to 3.476 $m^2.g^{-1}$ and 0.026 $cm^3\ g^{-1}$ with the introduction of ethylenediamine-glutaraldehyde on to MIL-101(Cr) surface. This indicates that ethylenediamine-glutaraldehyde took up the pores of the framework and hinder the diffusion and adsorption of N_2 (Abroudi et al., 2022).

Thermogravimetric analysis of MIL-101(Cr) and MIL-101(Cr)/EDGA were done to investigate their thermal stability (Fig. 3(d)). Two degradation steps were observed in both materials as depicted by the TGA plots in Fig. 3(d). The results were supported by differential thermal analysis (DTA) curves seen in Fig. 4(a)-(c) for MIL-101(Cr) and MIL-101 (Cr)/ED-GA. The TGA in Fig. 2(d) and DTA (Fig. 4(c)) comparison thermograms showed an enhancement in the thermal stability of MIL-101(Cr)/ED-GA. The TGA and DTA were supported by DSC curves which displayed endothermic peaks at 100 °C for water loss and exothermic peaks at 400 °C (MIL-101(Cr)) and 480 °C (MIL-101(Cr)/ED-GA) for degradation of the framework (Fig. 4(d)). The curves exhibited an intense exothermic peak at 92 °C for crystallization transition with changes in enthalpy (ΔH) of 2.46 and 2.82 kJ g^{-1} for MIL-101(Cr) and

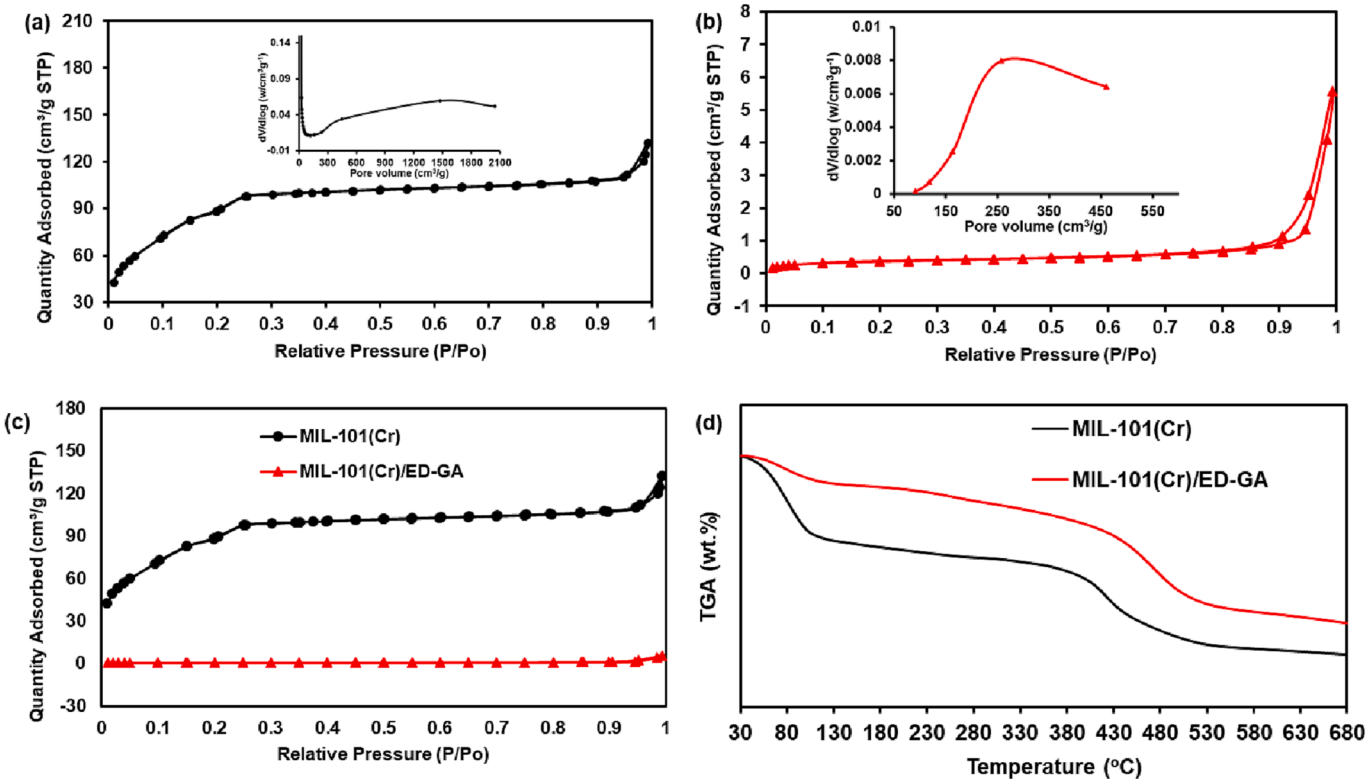

Fig. 3. BET measurement of (a) MIL-101 and (b) MIL-101(Cr)/ED-GA (inset: Pore diameter measurement). (c) Comparison BET isotherms and (d) TGA curves of MIL-101(Cr) and MIL-101(Cr)/ED-GA.

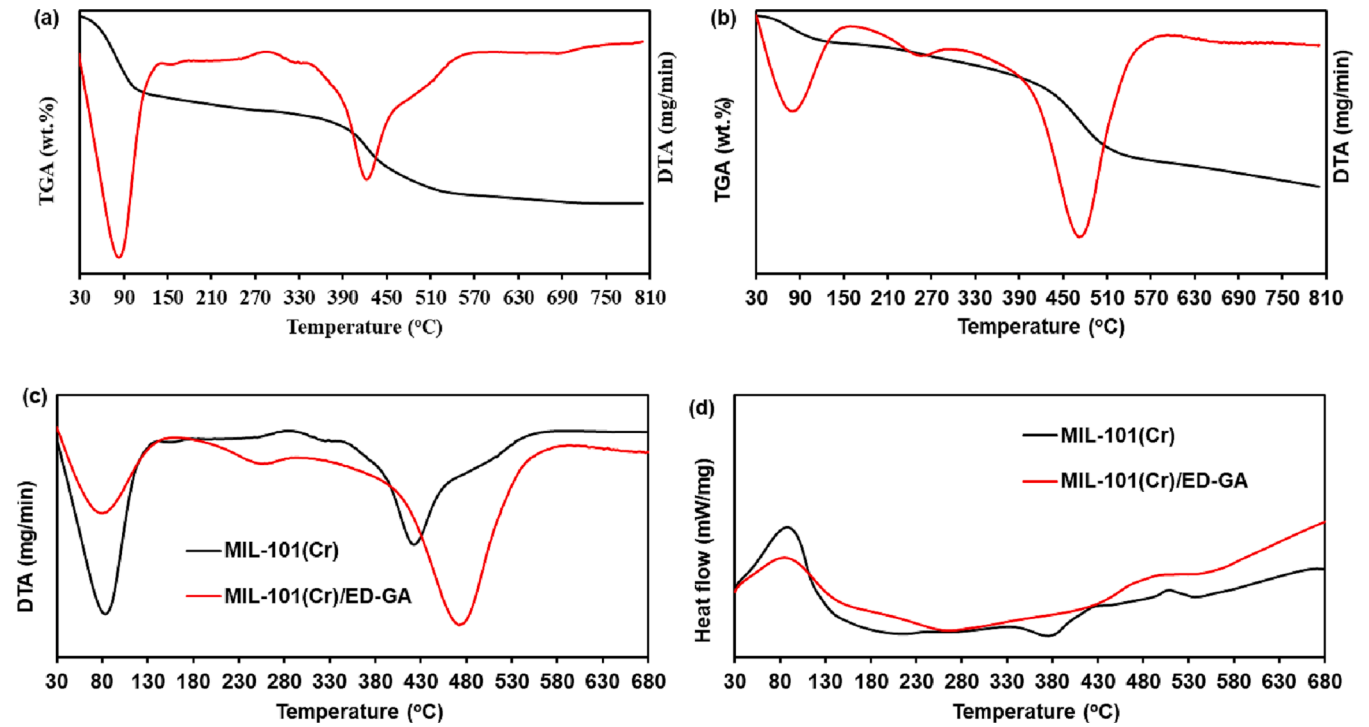

Fig. 4. TGA/DTA curves of (a) MIL-101(Cr), and (b) MIL-101(Cr)/ED-GA. (c) DTA and (d) DSC of MIL-101 and MIL-101(Cr)/ED-GA.

MIL-101(Cr)/ED-GA, respectively. The endothermic peak in MIL-101 (Cr)/ED-GA was detected at 272 °C with ΔH of 0.821 kJ g^{-1} for disintegration of ED and glutaraldehyde on the surface whereas MIL-101(Cr) had an endothermic peak at 382 °C with ΔH = 0.782 kJ g^{-1} for degradation of organic linker (Lim et al., 2020). In addition, there were small exothermic peaks at around 500 °C with ΔH = 0.789 and 2.00 kJ g^{-1} for MIL-101(Cr) and MIL-101(Cr)/ED-GA, respectively.

3.2. Morphological characterizations

The SEM image of the MIL-101(Cr) in Fig. 5(a) possessed discrete octahedron shapes with clear edges and corners, consistent with previous reports (Luo et al., 2015). Most crystals were made of uniform surface morphologies and some are split or lack angles. The octahedron shapes had a smooth surface with the majority of the particles having a size of 100–40 nm (Fig. 5(b)). The EDS spectrum of the MIL-101(Cr) presented in Fig. 5(c) revealed that the sample is composed of C, O, and Cr (the presence of small peaks of Al is accredited to the aluminium grid used SEM preparation procedure). The inset in Fig. 5(c) showed the relative contents of C, O, and Cr in the MIL-101(Cr) which were determined to be about 77.6, 20.1, and 1.4 at.%, respectively. The SEM image of the MIL-101(Cr)/ED-GA in Fig. 5(d) clearly demonstrated that its shape and morphology are similar to those of the MIL-101(Cr) with some increment in large particle size (Fig. 5(e)). Endorsing that the crystalline structure of MIL-101(Cr) r unchanged after incorporating ED and GA as seen in the XRD above. Nonetheless, the structural porosity of MIL-101 (Cr) decreased after the incorporation of GA due to the growth of the polymer chain with ED and GA. Fig. 5(f) and Fig. 6 shows the EDS spectrum and representative images of the MIL-101(Cr)/ED-GA with corresponding elemental mappings. The presence of C, O, Cr, and N elements was observed in the EDS spectrum in Fig. 5(f).

The system of spectral lines for distribution of elements in EDS is unique and characteristic for each element and therefore, can be used to study the chemical composition of micro-samples. It should be noted that the atoms, for instance carbon, nitrogen and oxygen as shown in Figs. 5 and 6, they have only two shells filled with electrons. The emissions in EDS for these atoms are only from the K series. Therefore, the excitation energy of the K series for such elements is very small, resulting in all peaks are overlapping in the low-resolution portion at low energy of EDS spectrum. On the other hand, chromium consists of the K, L, M and N series. The distribution of Cr showed distinct characteristic peaks of Kα and L series with clear chromium spectral lines at both low and high energy level of the EDS. As presented in Fig. 6(a-h), the corresponding elemental mapping distributions also showed the existence of C, O, Cr, and N elements. The EDS technique is mostly used for qualitative analysis of materials but is capable of providing semi-quantitative results as well. Herein the experimental values to compare with the theoretical composition of standard MIL-101 functionalized with ED followed by grafting with GA. The estimated molecular formula of $Cr_3C_{60}O_{20}N_6$, the presence of hydrogen was ignored because it can not be detected by EDS. The theoretical composition was determined to be 12.19, 56.25, 25.00 and 6.56 wt% for Cr, C, O, and N element, respectively. The experimental composition as shown in Fig. 6 (h) was 5.92 wt% for Cr, 67.49 wt% for C, 23.58 wt% for O and 3.01 wt % for N. There was slightly different to the theoretical composition due to the semi-quantitative analysis using EDS. Remarkably, the atomic percentage for theoretical and experimental values were almost similar. For example, the chromium was found to be 3.31 At.% using EDS which was in agreement with the theoretical one of 3.37 At.% and nitrogen measured to be 8.84 At.% as compared to the theoretical composition of 6.74 At.%. This behaviour of high N content in term of atomic percentage was expected. The estimated molecular formula of the prepared material has two nitrogen of ED where one ED molecule binds with one open Cr site making six N to three Cr. From the EDS spectra and maps, it was seen that the elements are uniformly distributed over the MIL-101 (Cr)/ED-GA, confirming the homogeneity of the samples. The increase in the amount of C and N elements was due to the presence of ED and GA chain, thus confirming the uniform incorporation of ED and GA chain into the porous MIL-101(Cr) framework. The obtained morphological and structural characterizations of the synthesized materials indicated the presence of reactive species in the MIL-101(Cr)/ED-GA. This clearly suggests that the adsorption of Pd^{2+} and Pt^{4+} ions on the MIL-101(Cr)/ED-GA will arise from the electrostatic interaction of these ions with the reactive species on the surface. Hence in this work, the removal of Pd^{2+} and Pt^{4+} ions from contaminated aqueous solutions using MIL-101(Cr)/ED-GA as a novel adsorbent was investigated.

3.3. Computation studies

The atomic structures of Pt and Pd adsorption on MIL-101(Cr)/ED-GA at various sites are shown in Fig. 7, to investigate the interaction behaviour of Pd and Pt ions with MIL-101(Cr)/ED-GA. This was

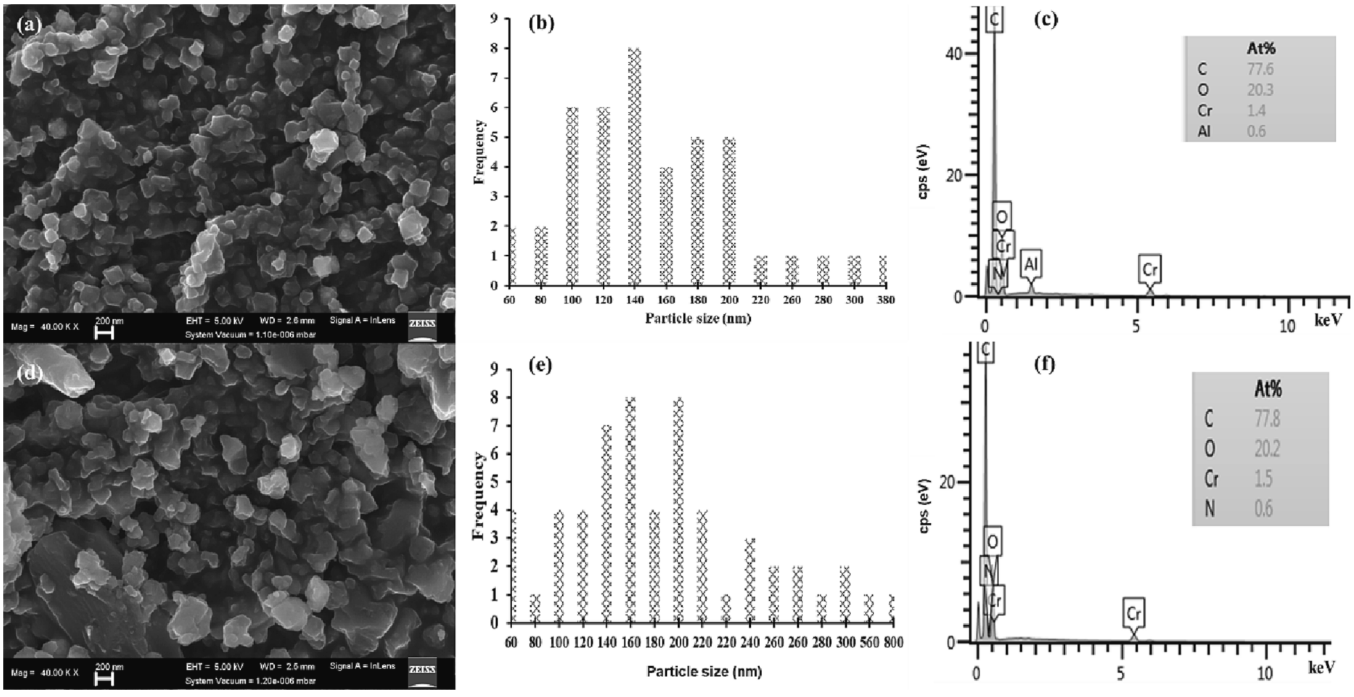

Fig. 5. (a) SEM image, (b) particle size distribution and (c) EDS spectrum of MIL-101(Cr) MIL-101(Cr)/ED-GA. (d) SEM image, (e) particle size distribution and (f) EDS spectrum of MIL-101(Cr)/ED-GA (Inset: elemental analysis in atomic percentage).

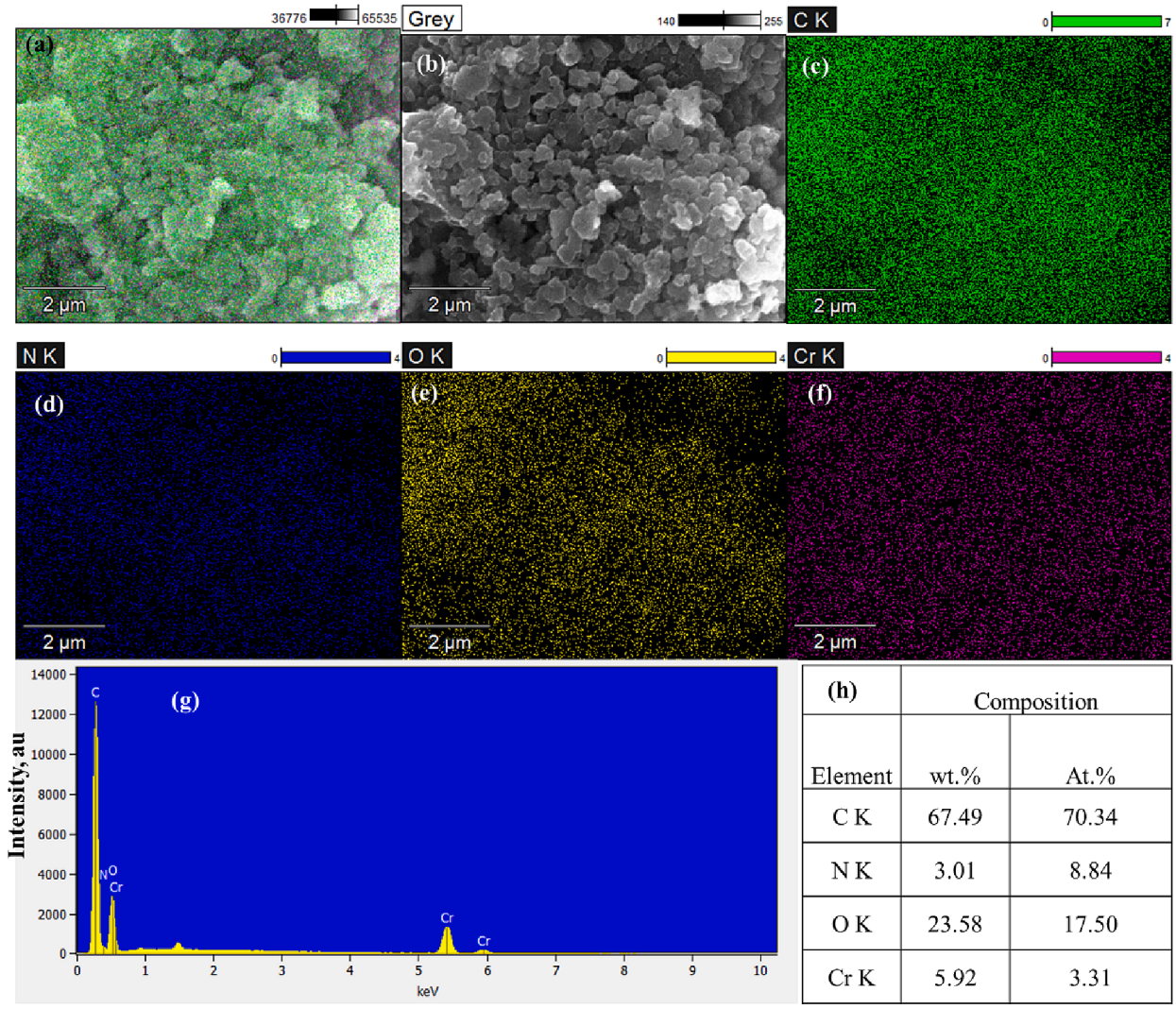

(h)	Composition	
Element	wt.%	At.%
C K	67.49	70.34
N K	3.01	8.84
O K	23.58	17.50
Cr K	5.92	3.31

Fig. 6. Elemental mapping of MIL-101(Cr)/ED-GA, (a) light, and (b) grey images, (c)-(f) mapping image of carbon, nitrogen, oxygen, and chromium elements, respectively. (g) EDS spectrum and (h) tabulated atomic weight percentages of MIL-101(Cr)/ED-GA.

established by the investigation of the adsorption configuration and energy characteristics. Different adsorption sites were considered for both ions to determine the strongest interaction. All the adsorption energies were found to be negative except for Pt interaction with the C atom at GA sites. For $E_{ads.} < 0$ implies that the interaction of Pd or Pt is a thermodynamically favourable and spontaneous reaction, and vice versa. In addition, a relatively large negative adsorption energy value implies a stronger adsorbing strength and more stability. The adsorption energy of Pd on N atoms (ED) was found to be −2851.29 kJ mol^{-1} while the Pt was adsorbed with $E_{ads.}$ = -291.431 kJ mol^{-1}. The bond lengths of 2.828 Å and 2.854 Å for Pd-N and Pt-N, respectively. The adsorption energy of Pd ion on the O atom GA site is high (-36.75 kJmol^{-1}), which is more than two times that of the Pt adsorption (-13.12 kJ mol^{-1}). This indicates that the adsorption of Pd or Pt on the N atom (ED) and O atom (GA) is energetically stable. This suggests that the adsorption of Pd or Pt ions on MIL-101(Cr)/ED-GA is more favourable and encourages the experimental investigations as given in the next section.

3.4. Adsorption results

3.4.1. Influence of pH and adsorbent dosage

The original solution pH directly influences the intake of Pd^{2+} and Pt^{4+} ions by MIL-101(Cr)/ED-GA. Depending on the pH value, the reactive groups can either be protonated or deprotonated to electrostatically interact with metal ions that are present in the solution (Wang et al., 2017). Fig. 8(a) depicts the influence of solution pH on the uptake of Pd^{2+} and Pt^{4+} ions by MIL-101(Cr)/ED-GA. The results show that the removal percentage for both Pd^{2+} and Pt^{4+} increased with increasing pH from 1.0 to 4.0 and decreased beyond 4.0. The optimum pH value was obtained as 3.0 for Pd^{2+} and 4.0 for Pt^{4+}. This behavior is attributed to the higher degree of protonation occurring in acidic media on the N and O of the amide groups on the MIL-101(Cr)/ED-GA surface as shown in Equations (5) and (6) (Fujiwara et al., 2007):

$$O = CH - NH + H^+ + Cl^- \rightarrow O = CH - NH_2^+ + Cl^- \quad (5)$$

$$HN - CH = O + H^+ + Cl^- \rightarrow HO - CH = NH^+ + Cl^- \quad (6)$$

Moreover, in lower pH values of HCl the dominating species of the PGMs are anionic chlorocomplexes which can interact with the MIL-101 (Cr)/ED-GA through electrostatic interaction with the protonated amide groups through the mechanisms shown in Equation ((7)–(10)) (Zhou et al., 2010):

$$2RNH_2^+Cl^- + PtCl_6^{2-} \leftrightarrow \left(RNH_2^+\right)_2 PtCl_6^{2-} + 2Cl^- \quad (7)$$

$$2RNH^+Cl^- + PtCl_6^{2-} \leftrightarrow (RNH^+)_2 PtCl_6^{2-} + 2Cl^- \quad (8)$$

$$2RNH_2^+Cl^- + PdCl_4^{2-} \leftrightarrow \left(RNH_2^+\right)_2 PdCl_4^{2-} + 2Cl^- \quad (9)$$

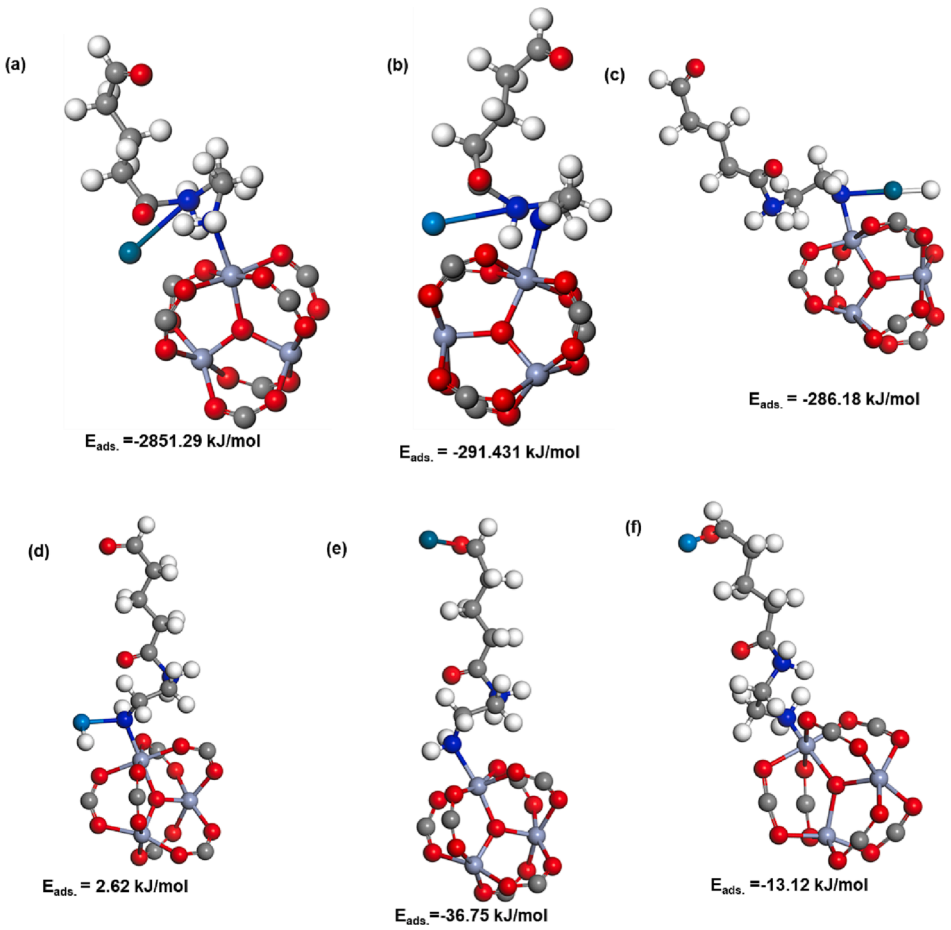

Fig. 7. Depicts the atomic structures and adsorption energies for Pd and Pt adsorption on MIL-101(Cr)/ED-GA;: (a) Pd-N1 on the Cr site, (b) Pt-N1 on the Cr site, (c) Pd-N2 of the amide bond, (d) Pt- N2 of the amide bond, (e) Pd- O of the GA, (f) Pt- O of the GA. Both Pd and Pt ions are depicted by the green atom in each structure.

$$2RNH^{+}Cl^{-} + PdCl_4^{2-} \leftrightarrow (RNH^{+})_2PdCl_4^{2-} + 2Cl^{-} \quad (10)$$

In addition, the pH drift method was employed to assess the point of zero charge (PZC) which was used to further deduce the possible interaction of MIL-101(Cr)/ED-GA with Pd^{2+} and Pt^{4+} ions as presented in Fig. 8(b). The attained values of PZC for Pd^{2+} and Pt^{4+} are 4.4 and 5.5, respectively. These results suggest that more adsorption is occurring below the PZC values as a result of electrostatic interaction between MIL-101(Cr)/ED-GA and metal ions. The results are in good correlation with the achieved optimum pH. Furthermore, the IR spectra of MIL-101 (Cr)/ED-GA after the adsorption of Pd^{2+} and Pt^{4+} were obtained and compared with the spectrum before adsorption and the results are depicted in Fig. 8(c). From the results, the interaction of Pd^{2+} with MIL-101(Cr)/ED-GA was noted by the reduction in the intensity of the C-N vibration at 1052 cm^{-1} and the disappearance of the N-H peaks at 1554 cm^{-1}. In the case of Pt^{4+}, the adsorption was confirmed by the broadening of the 1554 cm^{-1} peak as well as the enhancement of the peak at 1288 cm^{-1} which is due to the N-H vibration of the amide group. These results confirm the successful interaction of MIL-101(Cr)/ED-GA with Pd^{2+} and Pt^{4+} ions.

The influence of the amount of MIL-101(Cr)/ED-GA on the removal of Pd^{2+} and Pt^{4+} ions was investigated by varying the amount of adsorbent dose from 0.01 to 0.0.07 g for Pd^{2+} and 0.005–0.05 g for Pt^{4+} (Fig. 8(d)). The results for Pd^{2+} showed an increase in the removal percentage (%R) with an increase in the MIL-101(Cr)/ED-GA dose and the equilibrium was reached at 0.03 g. For Pt^{4+}, an increase in the %R was observed from 0.005 to 0.02 g of MIL-101(Cr)/ED-GA followed by a decrease as the dosage amount was increasing. The trends for Pt^{4+} removal by MIL-101(Cr)/ED-GA suggest that when more material is added there is a limited collision between adsorbate and adsorbent, hence in this work the optimum dose was taken as 0.02 g.

3.4.2. Adsorption isotherms

The equilibrium adsorption experiments for Pd^{2+} and Pt^{4+} ions removal by MIL-101(Cr)/ED-GA are shown in Fig. 9(a). The results revealed that the experimental adsorption capacity of MIL-101(Cr)/ED-GA is increasing with an increase in the initial concentrations from 50 to 400 mg L^{-1} for both Pd^{2+} and Pt^{4+} ions. To deduce the mode of adsorption, the obtained data were fit to the nonlinear Langmuir and Freundlich isotherm models given by the following Equations (11) and (12), respectively.

$$\frac{qe}{qm} = \frac{K_L C_e}{1 + K_L C_e} \quad (11)$$

$$qe = KFC_e^{1/n} \quad (12)$$

with q_m (mg g^{-1}) representing the Langmuir maximum adsorption capacity. The Langmuir and Freundlich constants are denoted by K_L (L mg^{-1}) and KF (mg g^{-1}), respectively. The results obtained from the nonlinear fittings revealed that both Pd^{2+} and Pt^{4+}adsorption data fitted well with the Langmuir isotherm model as the correlation coefficients R^2 values were closer to one than those predicted by the Freundlich nonlinear fittings (See Table 1). These observations were further supported by the linear fittings of the data to the two isotherm models which are given by Equations (13) and (14) and the results are shown in Fig. 9(b) and (c). The R^2 value predicted by the linear Langmuir model was 0.9821 for both Pd^{2+} and Pt^{4+} which was higher than 0.7913 and

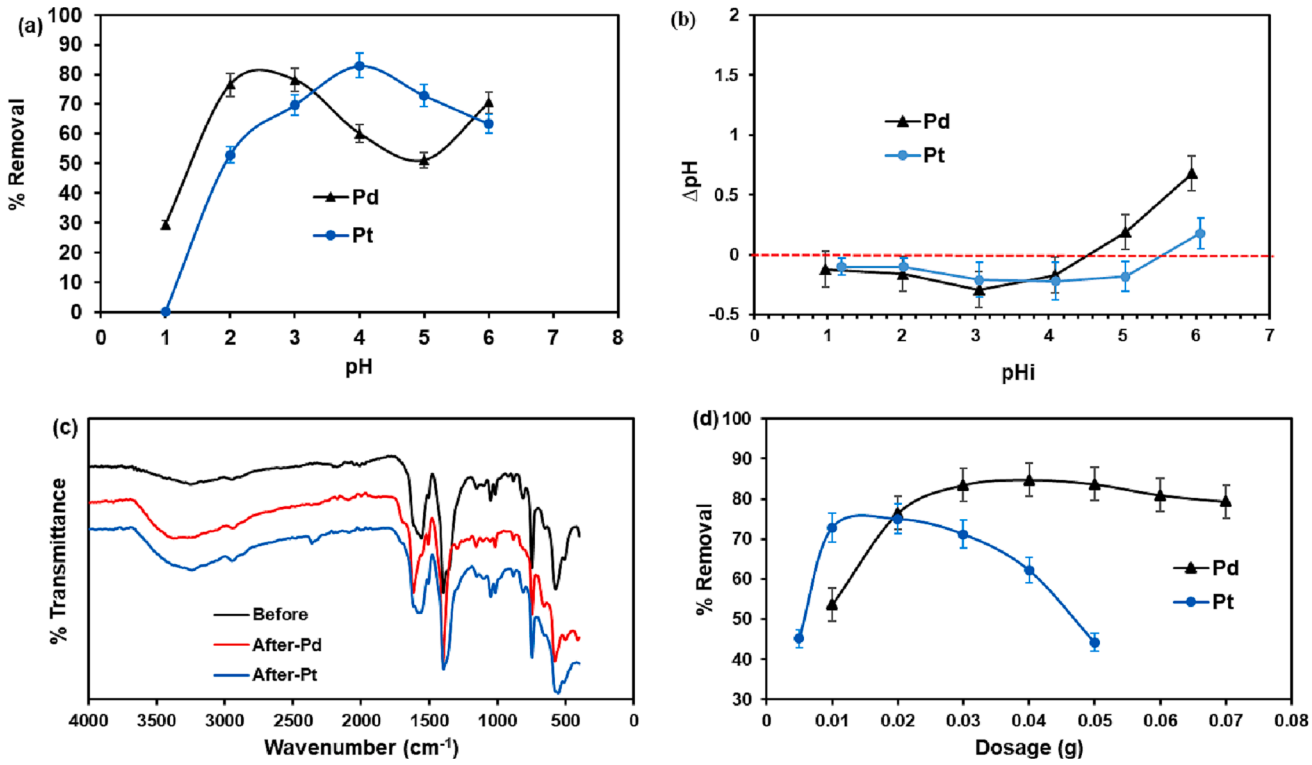

Fig. 8. (a) pH effect on the removal of Pd^{2+} and Pt^{4+} ions by MIL-101(Cr)/ED-GA (b) PZC of MIL-101(Cr)/ED-GA. (c) FTIR spectra of MIL-101(Cr)/ED-GA before and after Pd^{2+} and Pt^{4+} ions uptake. (d) MIL-101(Cr)/ED-GA dose effect on Pd^{2+} and Pt^{4+}adsorption.

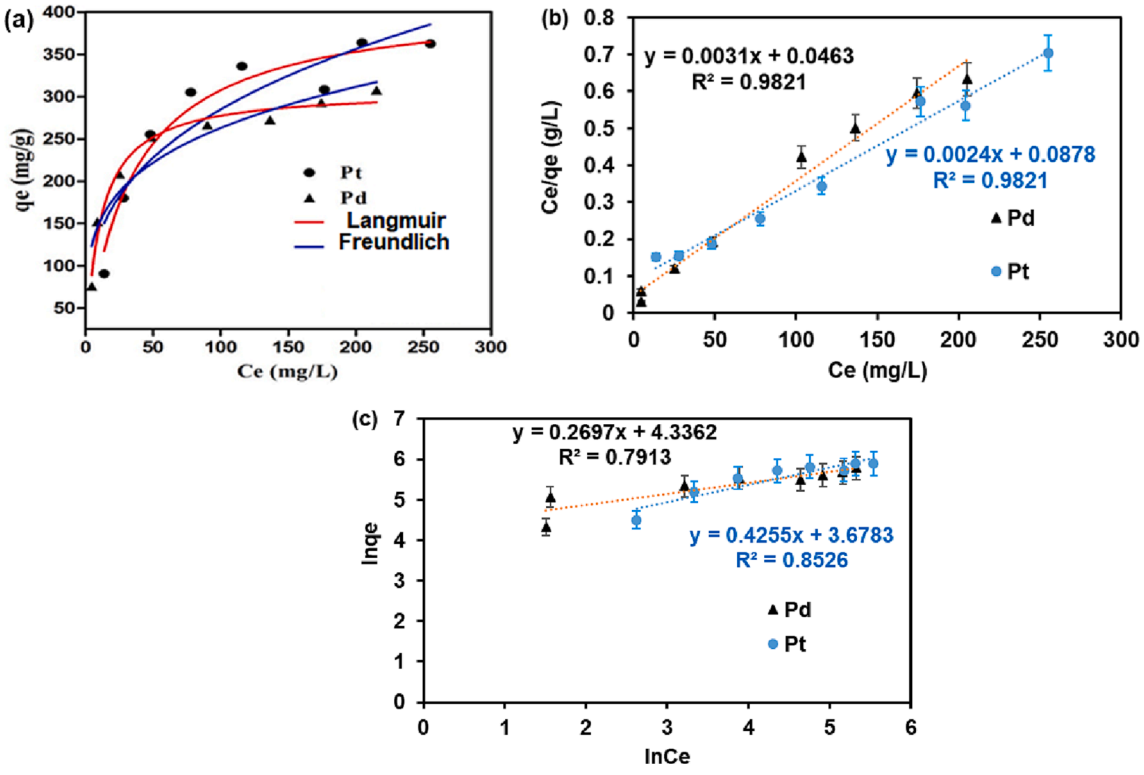

Fig. 9. (a) Equilibrium adsorption and nonlinear isotherm data for the removal of Pd^{2+} and Pt^{4+} ions by MIL-101(Cr)/ED-GA. (b) Langmuir isotherm linear curve (c) Linear curve of the Freundlich isotherm model.

0.8526 for Pd^{2+} and Pt^{4+}, respectively, which were depicted by the Freundlich model. This behavior suggests that the adsorption of Pd^{2+} and Pt^{4+} by MIL-101(Cr)/ED-GA is through a monolayer.

$$\frac{C_e}{q_e} = \frac{1}{qmK_L} + \frac{C_e}{qm} \tag{13}$$

Table 1
Isotherms data of MIL-101(Cr)/ED-GA after the adsorption of Pd^{2+} and Pt^{4+} metal ions.

Isotherm models$Pd^{2+}Pt^{4+}$		
	Pd^{2+}	Pt^{4+}
Langmuir		
Linear		
q_m	322.6	416.17
K_L	0.0670	0.0273
R_L	0.0695	0.1546
R^2	0.9821	0.9821
Non-linear		
Best-fit values		
q_m	308.3	414.4
K_L	0.08948	0.02875
Std. Error		
q_m	7.977	22.97
K_L	0.01165	0.005892
95 % Confidence Intervals		
q_m	288.8 to 327.8	358.2 to 470.6
K_L	0.06097 to 0.1180	0.01433 to 0.04316
Goodness of Fit		
Degrees of Freedom	6	6
R^2	0.9794	0.9513
Absolute Sum of Squares	906,1	3144
Sy.x	12.29	22.89
Number of points		
Analyzed	8	8
Freundlich		
Linear		
K_F	76.42	21.266
N	3.708	1.836
R^2	0.7913	0.8526
Non-linear		
Best-fit values		
K_F	85.29	64.48
N	4.09	3.1
Std. Error		
K_F	15.41	20.6
N	0.6522	0.6246
95 % Confidence Intervals		
K_F	47.58 to 123.0	14.08 to 114.9
N	2.495 to 5.686	1.572 to 4.628
Goodness of Fit		
Degrees of Freedom	6	6
R^2	0.9052	0.8539
Absolute Sum of Squares	4162	9443
Sy.x	26.34	39.67
Number of points		
Analyzed	8	8

$$\ln q_e = \ln K_F + \frac{1}{n} ln C_e \tag{14}$$

Furthermore, the maximum adsorption capacity (q_m) of the functionalized MIL-101(Cr)/ED-GA towards Pd^{2+} and Pt^{4+} ions were determined from the linear form of the Langmuir isotherm model and obtained as 322.6 mg/g for Pd^{2+} and 416.7 mg/g for Pt^{4+}. These results show that MIL-101(Cr)/ED-GA has a higher affinity for PGMs as the values are higher than those reported in the literature as shown in Table 2. Additionally, the Langmuir isotherm model is associated with a dimensionless parameter called the separation factor denoted by R_L. This constant assists in deducing the favorability of the adsorption process and is determined by the below Equation (15).

$$R_L = \frac{1}{1 + K_L C_0} \tag{15}$$

For the adsorption process to be favorable, the R_L values should be greater than zero but less than one ($0 < R_L > 0.1$). The calculated values suggest that the adsorption of Pd^{2+} and Pt^{4+} on the surface of MIL-101 (Cr)/ED-GA is favorable since $R_L = 0.0695$ and 0.1546 (see Table 1).

Table 2
A comparison of the adsorption capacity of Pd^{2+} and Pt^{4+} metal ions by MIL-101 (Cr)/ED-GA with reported literature.

Adsorbent	**Pt^{4+} q_m (mg/g)**	**Pd^{2+} q_m (mg/g)**	**Experimental conditions**	**Refs**
Calcined aluminum hydroxide gels	23.9	23.4	pH 5.0, 20 mg, 20 mg/L	(Fumihiko and Kawasaki, 2013)
ED/Chitosan NPs	171	138	pH 2.0, 50 mg, 60 mg/L	(Zhou et al., 2010)
bayberry tannin collagen fiber membrane	41.7	27.5	pH 3.0 and 4.0, 100 mg, 50 mg/L	(Ma et al., 2006)
mGO@SiO2@PPy-PTh	50	45	pH 4.5, 19 mg, 0.2 mg/L	(Jalilian et al., 2017)
GLA-PEI@ algal biomass beads	100	120	pH 2.5, 50 mg, 50 and 40 mg/L	(Wang et al., 2017)
L-lysine/Chitosan	129.26	109.47	pH 1.0 and 2.0, 100 mg, 100 mg/L	(Fujiwara et al., 2007)
MIL-101(Cr)–NH_2	140.7	277.6	pH 1.0, 10 mg, 200 mg/L	(Lim et al., 2020)
MIL-101(Cr)–NO_2	104.5	119.5	pH 1.0, 10 mg, 200 mg/L	(Lim et al., 2020)
quaternary ammonium-Zr^{4+} metal–organic resin	245.7	123.2	pH 7.5, 200 mg/L, 10 mg	(Chen et al., 2021)
Polystyrene nanofiber/EDAbead	7.4	4.3	pH 1.0, 10 mg/L, 150 mg	(Fayemi et al., 2013)
Glycine/chitosan resin	122.47	120.39	pH 2.0, 330 mg, 100 mg/L	(Ramesh et al., 2008)
MIL-101 (Cr)-GA	416.17	322.6	pH 3.0 and 4.0, 200 mg/L, 20 mg	This work

3.4.3. Adsorption kinetics

The influence of contact time on the adsorption of Pd^{2+} and Pt^{4+} metal ions by MIL-101(Cr)/ED-GA was also assessed in order to get an insight into the adsorption process. The experiments were conducted at an initial concentration of 100 mg L^{-1} at 25 °C for both Pd^{2+} and Pt^{4+}. From the results presented in Fig. 10(a), there is an increase in the adsorption capacity for both Pd^{2+} and Pt^{4+} ions with an increase in contact time. In addition, the MIL-101(Cr)/ED-GA demonstrated fast kinetics for the adsorption Pd^{2+} which reached equilibrium after 20 min as compared to the kinetics for Pt^{4+} which equilibrated after 60 min. The data obtained from kinetics experiments were then used to establish the rate of adsorption and other adsorption kinetics parameters, by fitting it to the nonlinear and linear forms of the pseudo-first-order (PFO) and the pseudo-second-order (PSO) kinetic models determined using the following Equations:

$$\frac{dqt}{dt} = k_1(q_e - q_t) \tag{16}$$

$$\frac{dqt}{dt} = k_2(q_e - q_t)^2 \tag{17}$$

$$\ln(q_e - q_t) = \ln{\cdot}q_e - k_1 t \tag{18}$$

$$\frac{t}{qt} = \frac{1}{k_2 q^2 t} + \frac{1}{q_e} t \tag{19}$$

where k_1 (min^{-1}) represents the PFO rate constant and k_2 (g mg^{-1} min^{-1}) denotes the PSO rate constant.

The experimental observations were supported by PSO rate constant k_2 values which were obtained as 2.603 x10^{-3} g mg^{-1} min^{-1} for Pd^{2+} and 3.46 × 10^{-4} g mg^{-1} min^{-1} for Pt^{4+} determined from the nonlinear fittings, respectively (see Table 3). The data was further fit to the linear

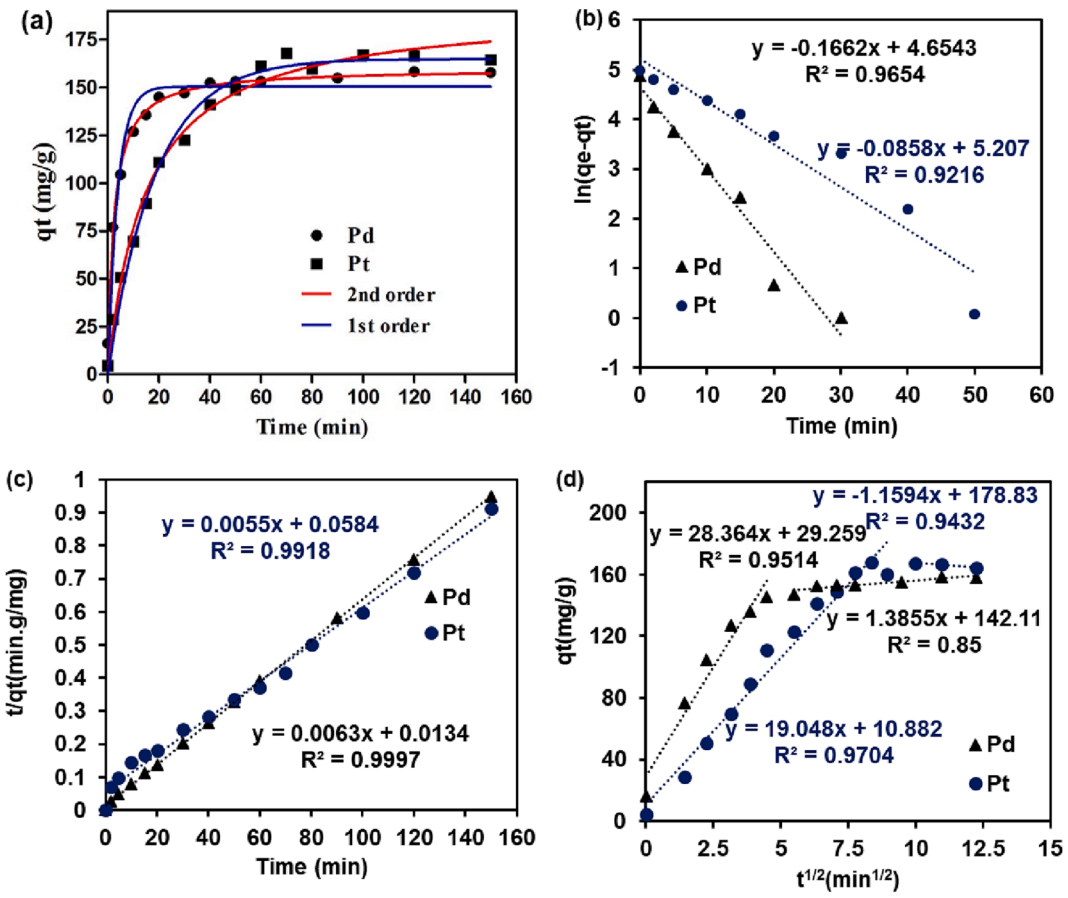

Fig. 10. (a) Kinetics experimental data and nonlinear fittings. Linear fitting of Pd^{2+} and Pt^{4+} data to the pseudo (b) 1st –order and (c) 2nd order. (d) Intra-particle diffusion model.

Table 3
Kinetics data on the adsorption of Pd^{2+} and Pt^{4+} ions by MIL-101 (Cr)/ED-GA.

Kinetic models	1st -order		2nd –order	
	Pt^{4+}	Pd^{2+}	Pt^{4+}	Pd^{2+}
Linear				
q_e	182.5	105.0	181.8	158.7
k_1 or k_2	0.0858	0.1662	0.001415	0.006168
R^2	0.9216	0.9654	0.9918	0.9997
Non-linear				
Best-fit values				
q_e	165	150.5	191.5	159.9
k_1 or k_2	0.05371	0.2576	0.000346	0.002603
Std. Error				
q_e	2.795	3.247	4.437	2.329
k_1 or k_2	0.003425	0.03484	0.00003838	0.000308
95% Confidence Intervals				
q_e	158.9 to 171.0	143.3 to 157.6	181.9 to 201.1	154.8 to 165.0
k_1 or k_2	0.04631 to 0.06110	0.1809 to 0.3343	$2.6x10^{-4}$ to $4.3x10^{-4}$	$1.9x10^{-3}$ to $3.3x10^{-3}$
Goodness of fit				
Degrees of Freedom	13	11	13	11
R^2	0.9877	0.9509	0.989	0.9847
Absolute Sum of squaresSquares	528.1	1018	474	316.1
Sy.x	6.373	9.619	6.038	5.361
# of points analyzed	15	13	15	13

pseudo 1st and 2nd order kinetic models (see Fig. 10(b) and (c)). The results showed a better fit of data to the 2nd order for both Pd^{2+} and Pt^{4+} adsorption by MIL-101(Cr)/ED-GA with the R^2 values of 0.9997 and 0.9918, respectively. This behavior implies that the rate-limiting step is the chemisorption mechanism wherein, the removal of Pd^{2+} and Pt^{4+} ions from an aqueous solution is through physicochemical interaction with the surface of the MIL-101(Cr)/ED-GA (Zhou et al., 2009); (Robati, 2013). The data was validated by fittings on the Weber and Morris intra-particle diffusion model given by Equation (20) (Maponya et al., 2020).

$$q_t = k_i t^{0.5} + C \quad (20)$$

with k_i (g $mg^{-1}(min^{-1})^{0.5}$) and C (mg g^{-1}) denoting the rate constant measured and intercept associated with the thickness of the boundary layer, respectively. As depicted in Fig. 10(d), the adsorption of both Pd^{2+} and Pt^{4+} ions by MIL-101(Cr)/ED-GA is controlled by two steps. Step one which is the intra-particle diffusion, it is the rate-limiting and is rapid for Pd^{2+} adsorption with $k_i = 28.36$ g $mg^{-1}(min^{-1})^{0.5}$than for Pt^{4+} where $k_i = 19.04$ g $mg^{-1}(min^{-1})^{0.5}$.

3.4.4. Selectivity and reusability tests

The selectivity of the adsorbent towards the targeted pollutant is a vital parameter in the adsorption process. For assessing the selectivity of the MIL-101(Cr)/ED-GA towards the uptake of Pd^{2+} and Pt^{4+} ions, the different molar ratios of Pd^{2+}/Pt^{4+} (25–100 mg L^{-1}) solutions were prepared and contacted with 25 mg of MIL-101(Cr)/ED-GA at a pH of 3.5 and a temperature of 25 °C for 24 h. From the acquired results represented by Fig. 11(a), MIL-101(Cr)/ED-GA showed the highest affinity towards the adsorption of Pd^{2+} than Pt^{4+}. The removal percentage of Pd^{2+} was still above 95 % after varying the concentration of Pt^{4+}.

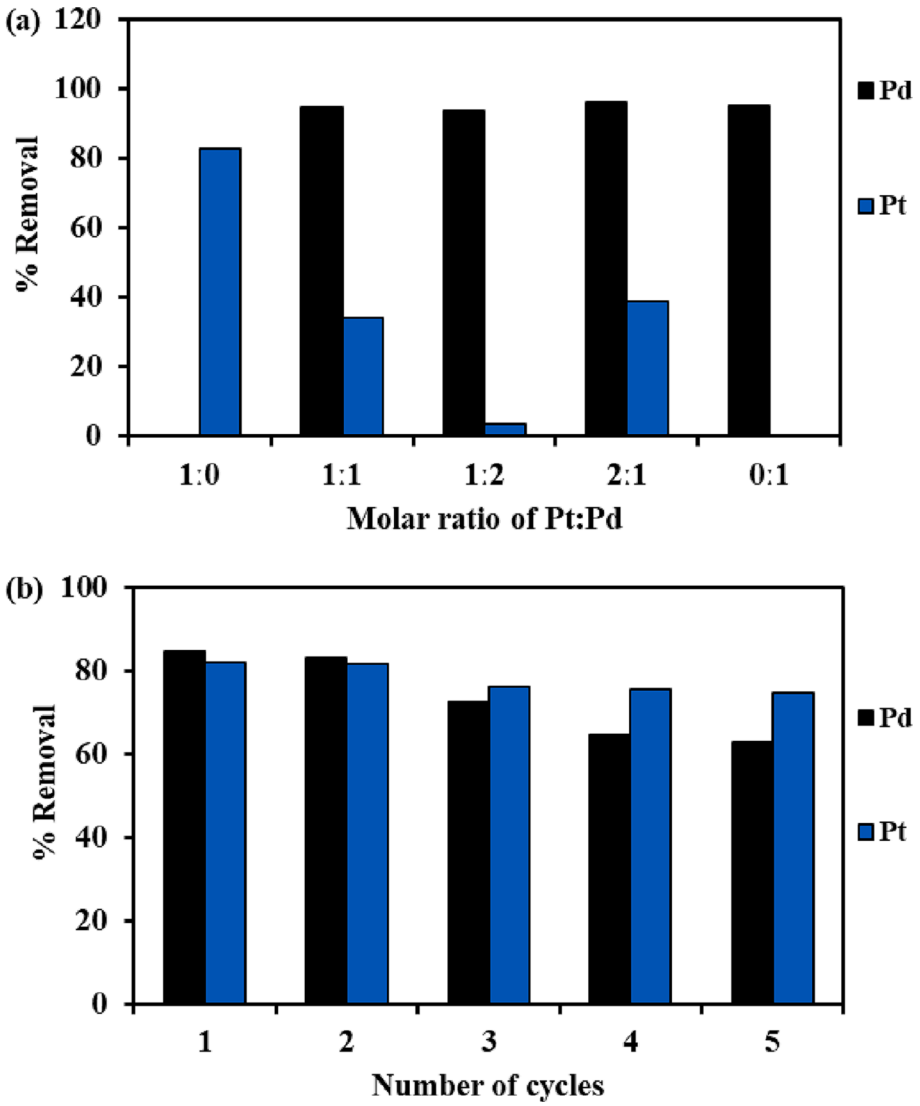

Fig. 11. (a) Selectivity test of MIL-101(Cr)/ED-GA towards Pd^{2+} and Pt^{4+} adsorption. (b) Reusability of MIL-101(Cr)/ED-GA.

Conversely, the removal percentage of Pd^{2+} ions demonstrated a significant decrease with an increase in the amount of Pd^{2+}. These results suggest that MIL-101(Cr)/ED-GA is more selective towards the adsorption of Pd^{2+} ions than Pt^{4+} and they are in good correlation with the kinetics data which revealed fast kinetic of Pd^{2+} ions.

In addition to the ideal properties of the adsorbent material, another aspect to consider is the regeneration and the reusability of the adsorbent. The reusability of the MIL-101(Cr)/ED-GA adsorbent was investigated for 5 consecutive cycles and regeneration was done using 6 M HCl. Fig. 10(b) revealed that the removal percentage for Pd^{2+} and Pt^{4+} ions by MIL-101(Cr)/ED-GA decreased with an increase in the number of cycles. This may be attributed to the over-oxidation of the ED and glutaraldehyde chain leading to the disruption of the active sites (Maponya et al., 2020). However, the removal percentage was still above 70% from the 3rd to the 5th cycle on the adsorption of Pt^{4+}. For the adsorption of Pd^{2+} ions, the removal reduced to <70 % starting from the 4th cycle. In addition to these preliminary results, the desorption procedure can further be investigated and improved to validate the potential utilization of the prepared MIL-101(Cr)/ED-GA material.

3.4.5. Structural stability

In order to evaluate the roles of the structural stability of the prepared MIL-101(Cr)/ED-GA in the adsorption process of Pd and Pt, FTIR and XRD analyses were carried before, after adsorption and desorption. The results are shown in Fig. 12. As can be seen from Fig. 12(a) and (b), beside the classical and well-known bands of C–O stretching vibrations and CN stretching of the amide bond, some broaden of bands appeared after adsorption which are very close to the observations made above. After desorption, the vibrations were similar to the FTIR of the adsorbent before adsorption indicating that the structural properties of the material were maintained. These observation was in agreement with the XRD before and after desorption which showed a related patterns as seen in Fig. 12(c) and (d) for Pd and Pt removal by MIL-101(Cr)/ED-GA, respectively.

4. Conclusion

In this work, the focus was on synthesizing MIL-101(Cr)/ED-GA to efficiently remove precious metal Pd^{2+} and Pt^{4+} ions from an aqueous solution. The successful synthesis of MIL-101(Cr)/ED-GA was confirmed by the FTIR with the appearance of the amide bond vibrations at 1554 and 1052 cm^{-1} owing to the interaction of ED and GA end. The results showed that more Pd^{2+} and Pt^{4+} ions were removable in acidic media whereby they exist as anion complexes. The isotherm data revealed that MIL-101(Cr)/ED-GA has a higher capacity for Pt^{4+} than Pd^{2+} with values of 416.17 and 322.6 mg g^{-1}, respectively. However, MIL-101

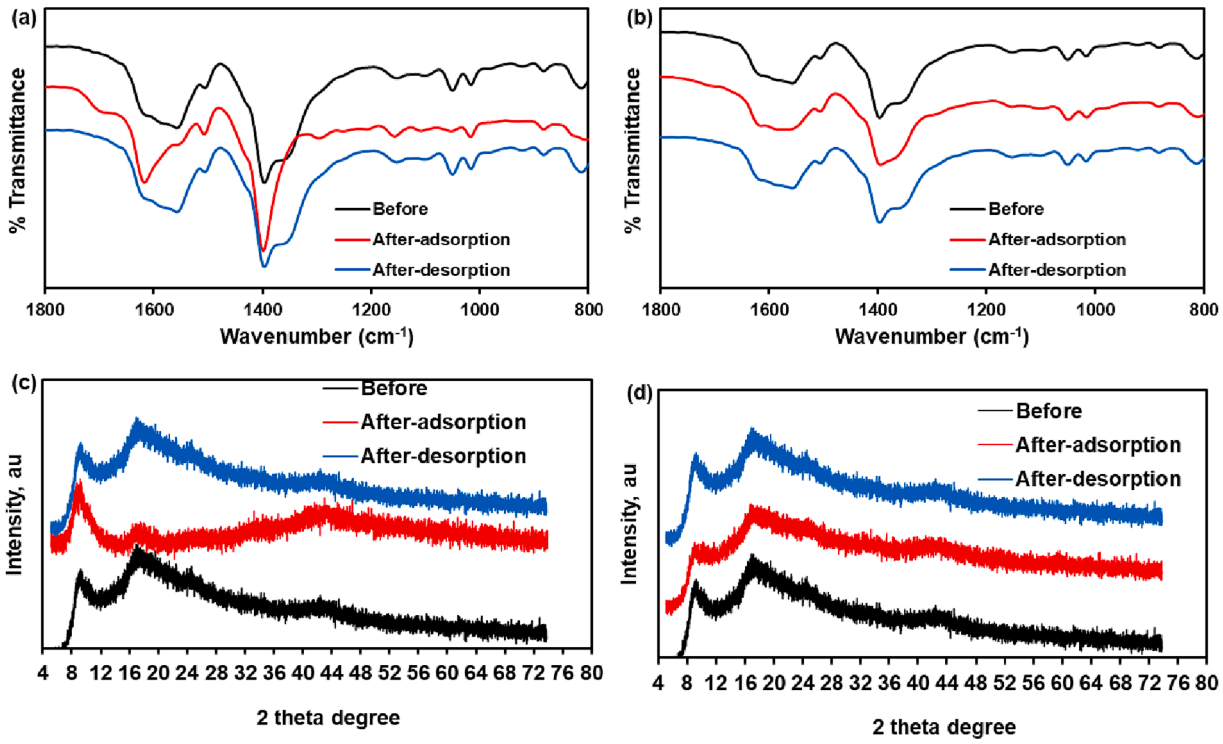

Fig. 12. FTIR spectra of MIL-101(Cr)/ED-GA of (a) Pd and (b) Pt before, after adsorption and desorption. XRD patterns of MIL-101(Cr)/ED-GA of (c) Pd and (d) Pt before, after adsorption and desorption.

(Cr)/ED-GA displayed higher affinity for Pd^{2+} since its removal % was more than 95%. Furthermore, the rate of Pd^{2+} adsorption by MIL-101 (Cr)/ED-GA was more rapid and resulted in the high selectivity of the ions in the presence of Pt^{4+}. In addition, DFT results showed that the adsorption of Pd^{2+} ions through the N atoms is more thermodynamically favoured than the adsorption of Pt^{4+}as given by the higher binding energy value of -2851.29 kJ mol^{-1}. Therefore, MIL-101(Cr)/ED-GA demonstrated great potential in terms of recovering both Pt^{4+} and Pd^{2+} from industrial wastewater.

Funding

KM and KDM would like to thank the financial support from the National Research Foundation (NRF) under the Thuthuka (UID Nos. 117727, and 118113) and the Competitive Support for Unrated Researchers (UID No. 138085) programmes.

CRediT authorship contribution statement

Thabiso C. Maponya: Methodology, Visualization, Investigation, Writing – original draft, Data Curation, Formal analysis, Validation, Software, Writing – review & editing. **Katlego Makgopa:** Supervision, Conceptualization, Resources, Funding acquisition, Project administration, Writing – review & editing. **Thabang R. Somo:** Data Curation, Formal analysis, Validation, Software, Writing – review & editing. **David M Tshwane:** Data Curation, Formal analysis, Validation, Software, Writing – review & editing. **Kwena D. Modibane:** Supervision, Conceptualization, Resources, Funding acquisition, Project administration, Writing – review & editing.

Declaration of Competing Interest

The authors declare that they have no known competing financial interests or personal relationships that could have appeared to influence the work reported in this paper.

Data availability

Data will be made available on request.

References

Abroudi, M., Tadjarodi, A., Rezvani, Z., Mollahosseini, A., Ahmadian, S.M.S., 2022. Synthesis and characterization of Pd nanoparticles anchored on MIL 101 (Cr) as a novel and recyclable catalyst for the Suzuki cross-coupling reactions. Microporous Mesoporous Mater. 331, 111599. https://doi.org/10.1016/j.micromeso.2021.111599.

Anılır, G., Sert, E., Yılmaz, E., Atalay, F.S., 2020. Preparation and performance of functionalized metal organic framework, MIL-101, for Knoevenagel reaction. J. Solid State Chem. 283, 121138. https://doi.org/10.1016/j.jssc.2019.121138.

Arora, R., 2019. Adsorption of heavy metals-a review. Mater. Today Proc. 18 (1), 4745–4750. https://doi.org/10.1016/j.matpr.2019.07.462.

Burrows, A.D., Jiang, D., Keenan, L.L., Burrows, A.D., Edler, K.J., 2012. Synthesis and post-synthetic modification of MIL-101 (Cr) -NH_2 via a tandem diazotisation process. Chem Comm. 48 (99), 99–102. https://doi.org/10.1039/c2cc36344e.

Chen, M., Li, S., Jin, C., Shao, M., Huang, Z., Xie, X., 2021. Removal of metal-cyanide complexes and recovery of Pt (II) and Pd (II) from wastewater using an alkali – tolerant metal-organic resin. *J. Hazard. Mater.* 406 (October 2020), 124315. https://doi.org/10.1016/j.jhazmat.2020.124315.

Dabrowski, A., 2001. Adsorption - From theory to practice. Adv. Colloid Interface Sci. 93 (1–3), 135–224. https://doi.org/10.1016/S0001-8686(00)00082-8.

Fajar, A.T.N., Hanada, T., Goto, M., 2021. Recovery of platinum group metals from a spent automotive catalyst using polymer inclusion membranes containing an ionic liquid carrier. J. Memb. Sci. 629 (February), 119296 https://doi.org/10.1016/j.memsci.2021.119296.

Fayemi, O.E., Ogunlaja, A.S., Kempgens, P.F., Antunes, E., Torto, N., Nyokong, T.T., Tshentu, Z.R., 2013. Adsorption and separation of platinum and palladium by polyamine functionalized polystyrene-based beads and nanofibers. Miner. Eng. 53, 256–265. https://doi.org/10.1016/j.mineng.2013.06.006.

Fujiwara, K., Ramesh, A., Maki, T., Hasegawa, H., Ueda, K., 2007. Adsorption of platinum IV), palladium(II) and gold(III) from aqueous solutions onto l -lysine modified crosslinked chitosan resin. J. Hazard. Mater. 146, 39–50. https://doi.org/10.1016/j.jhazmat.2006.11.049.

Fumihiko, Q., Kawasaki, N., 2013. Adsorption of Pt (IV) and Pd (II) by calcined dried aluminum hydroxide gel from aqueous solution system. J. Environ. Chem. Eng. 1, 1013–1019. https://doi.org/10.1016/j.jece.2013.08.011.

Göksungur, Y., Üren, S., Güvenç, U., 2005. Biosorption of cadmium and lead ions by ethanol treated waste baker's yeast biomass. Bioresour. Technol. 96 (1), 103–109. https://doi.org/10.1016/j.biortech.2003.04.002.

Hasan, Z., Choi, E.J., Jhung, S.H., 2013. Adsorption of naproxen and clofibric acid over a metal–organic framework MIL-101 functionalized with acidic and basic groups. Chem. Eng. J. 219, 537–544. https://doi.org/10.1016/j.cej.2013.01.002.

Hu, T., Jia, Q., He, S., Shan, S., Su, H., Zhi, Y., He, L., 2017. Novel functionalized metal-organic framework MIL-101 adsorbent for capturing oxytetracycline. J. Alloys Compd. 727, 114–122. https://doi.org/10.1016/j.jallcom.2017.08.116.

Jacob, K.T., Raj, S., Rannesh, L., 2007. Vegard 's law: a fundamental relation or an approximation? Int. J. Mater. Res. 98, 776–779. https://doi.org/10.3139/146.101545.

Jalayeri, H., Aprea, P., Caputo, D., Peluso, A., Pepe, F., 2020. Synthesis of amino-functionalized MIL-101(Cr) MOF for hexavalent chromium adsorption from aqueous solutions. Environ. Nanotechnol. Monit. Manag. 14 (February), 100300 https://doi.org/10.1016/j.enmm.2020.100300.

Jalilian, N., Ebrahimzadeh, H., Asgharinezhad, A.A., 2017. Extraction and determination of trace amounts of gold (III), palladium (II), platinum (II) and silver (I) with the aid of a magnetic nanosorbent made from $Fe_3{}_O4$ -decorated and silica-coated graphene oxide modified with a polypyrrole-polythiophe. Microchim. Acta 184, 2191–2200. https://doi.org/10.1007/s00604-017-2170-y.

Leng, K., Sun, Y., Li, X., Sun, S., Xu, W., 2016. Rapid synthesis of metal − organic frameworks MIL-101(Cr) without the addition of solvent and hydrofluoric acid. Cryst. Growth Des. 101, 1168–1171. https://doi.org/10.1021/acs.cgd.5b01696.

Lim, C., Lin, S., Yun, Y., 2020. Highly e ffi cient and acid-resistant metal-organic frameworks of MIL-101 (Cr) -NH2 for Pd(II) and Pt(IV) recovery from acidic solutions: adsorption experiments , spectroscopic analyses , and theoretical computations. *J. Hazard. Mater.* 387 (August 2019), 121689. https://doi.org/10.1016/j.jhazmat.2019.121689.

Lim, C.R., Lin, S., Yun, Y.S., 2020. Highly efficient and acid-resistant metal-organic frameworks of MIL-101(Cr)-NH2 for Pd(II) and Pt(IV) recovery from acidic solutions: adsorption experiments, spectroscopic analyses, and theoretical computations. *J. Hazard. Mater.* 387 (November 2019), 121689. https://doi.org/10.1016/j.jhazmat.2019.121689.

Lin, S., Bediako, J.K., Song, M., Kim, J., 2019. Metal organic frameworks using central composite design for synthesis Effective recovery of Pt (IV) from acidic solution by a defective metal-organic frameworks using central. ACS Sustain. Chem. Eng. 7, 7510–7518. https://doi.org/10.1021/acssuschemeng.8b04637.

Lin, S., Zhao, Y., Bediako, J.K., Cho, C.-W., Sarkar, A.K., Lim, C.-R., Yun, Y.-S., 2019. Structure-controlled recovery of palladium (II) from acidic aqueous solution using metal-organic frameworks of MOF-802, UiO-66 and MOF-808. Chem. Eng. J. 362, 280–286. https://doi.org/10.1016/j.cej.2019.01.044.

Luo, X., Ding, L., Luo, J., 2015. Adsorptive removal of Pb(II) ions from aqueous samples with amino-functionalization of metal-organic frameworks MIL-101(Cr). J. Chem. Eng. Data 60 (6), 1732–1743. https://doi.org/10.1021/je501115m.

Luo, X., Shen, T., Ding, L., Zhong, W., Luo, J., Luo, S., 2016. Novel thymine-functionalized MIL-101 prepared by post-synthesis and enhanced removal of Hg^{2+} from water. J. Hazard. Mater. 306, 313–322.

Ma, H., Liao, X., Liu, X., Shi, B., 2006. Recovery of platinum (IV) and palladium (II) by bayberry tannin immobilized collagen fiber membrane from water solution. J. Membr. Sci. 278, 373–380. https://doi.org/10.1016/j.memsci.2005.11.022.

Mabokela, T.E., Somo, T.R., Maponya, T.C., Hato, M.J., Makhado, E., Makgopa, K., Modibane, K.D., 2022. Dynamic carbon dioxide uptake capacity of metal organic framework using thermogravimetrical evaluation at different CO_2 pressure. Mater. Lett. 317, 132086. https://doi.org/10.1016/j.matlet.2022.132086.

Makhafola, M.D., Modibane, K.D., Ramohlola, K.E., Maponya, T.C., Hato, M.J., Makgopa, K., Iwuoha, E.I., 2021. Palladinized graphene oxide-MOF induced coupling of Volmer and Heyrovsky mechanisms, for the amplification of the electrocatalytic efficiency of hydrogen evolution reaction. Sci. Rep. 11 (1), 1–16. https://doi.org/10.1038/s41598-021-96536-9.

Maponya, T.C., Ramohlola, K.E., Kera, N.H., Modibane, K.D., Maity, A., Katata-Seru, L. M., Hato, M.J., 2020. Influence of magnetic nanoparticles on modified polypyrrole/m-phenylediamine for adsorption of Cr(VI) from aqueous solution. Polymers (Basel) 12 (3), 1–17. https://doi.org/10.3390/polym12030679.

Mashao, G., Ramohlola, K.E., Mdluli, S.B., Monama, G.R., Hato, M.J., Makgopa, K., Molapo, K.M., Ramoroka, M.E., Iwuoha, E.I., Modibane, K.D., 2019. Zinc-based zeolitic benzimidazolate framework/polyaniline nanocomposite for electrochemical sensing of hydrogen gas. Mater. Chem. Phys. 230, 287–298. https://doi.org/10.1016/j.matchemphys.2019.03.079.

Modrow, A., Zargarani, D., Herges, R., Stock, N., 2012. Introducing a photo-switchable azo-functionality inside Cr-MIL-101-NH_2 by covalent post-synthetic modification. Dalt. Trans. 41 (28), 8690–8696. https://doi.org/10.1039/c2dt30672g.

Monama, G.R., Hato, M.J., Ramohlola, K.E., Maponya, T.C., Mdluli, S.B., Molapo, K.M., Modibane, K.D., Iwuoha, E.I., Makgopa, K., Teffu, M.D., 2019. Hierarchiral 4-tetra-nitro copper(II)phthalocyanine based metal organic framework hybrid composite with improved electrocatalytic efficiency towards hydrogen evolution reaction. Results Phys. 15 (April), 102564 https://doi.org/10.1016/j.rinp.2019.102564.

Nikoloski, A.N., Ang, K., Li, D., 2015. Hydrometallurgy Recovery of platinum, palladium and rhodium from acidic chloride leach solution using ion exchange resins. Hydrometallurgy 152, 20–32. https://doi.org/10.1016/j.hydromet.2014.12.006.

Ragheb, E., Shamsipur, M., Jalali, F., Mousavi, F., 2022. Modified magnetic-metal organic framework as a green and efficient adsorbent for removal of heavy metals. J. Environ. Chem. Eng. 10 (2), 107297 https://doi.org/10.1016/j.jece.2022.107297.

Ramesh, A., Hasegawa, H., Sugimoto, W., Maki, T., Ueda, K., 2008. Adsorption of gold (III), platinum (IV) and palladium (II) onto glycine modified crosslinked chitosan resin. Bioresour. Technol. 99, 3801–3809. https://doi.org/10.1016/j.biortech.2007.07.008.

Ren, J., Dyosiba, X., Musyoka, N.M., Langmi, H.W., North, B.C., Mathe, M., Onyango, M. S., 2016. Green synthesis of chromium-based metal-organic framework (Cr-MOF) from waste polyethylene terephthalate (PET) bottles for hydrogen storage applications. Int. J. Hydrogen Energy 41 (40), 18141–18146. https://doi.org/10.1016/j.ijhydene.2016.08.040.

Robati, D., 2013. Pseudo-second-order kinetic equations for modeling adsorption systems for removal of lead ions using multi-walled carbon nanotube. J Nanostruct Chem. 3, 3–8. https://doi.org/10.1186/2193-8865-3-55.

Shafiei, M., Alivand, M.S., Rashidi, A., Samimi, A., Mohebbi-Kalhori, D., 2018. Synthesis and adsorption performance of a modified micro-mesoporous MIL-101(Cr) for VOCs removal at ambient conditions. Chem. Eng. J. 341, 164–174. https://doi.org/10.1016/j.cej.2018.02.027.

Snyders, C.A., Bradshaw, S.M., Akdogan, G., Eksteen, J.J., 2014. The effect of temperature, cyanide and base metals on the adsorption of Pt, Pd and Au onto activated carbon. Hydrometallurgy 149, 132–142. https://doi.org/10.1016/j.hydromet.2014.07.012.

Somo, T.R., Davids, M.W., Lototskyy, M.V., Hato, M.J., Modibane, K.D., 2021. Improved hydrogenation kinetics of $TiMn_{1.52}$Alloy coated with palladium through electroless deposition. Mater. 14, 1833. https://doi.org/10.3390/ma14081833.

Sun, Y., Zheng, L., Yang, Y., Qian, X., Fu, T., Li, X., Yang, Z., Yan, H., Cui, C., Tan, W., 2020. Metal–organic framework nanocarriers for drug delivery in biomedical applications. Nano-Micro Lett. 12 (1), 1–29. https://doi.org/10.1007/s40820-020-00423-3.

Tang, J., Chen, Y., Wang, S., Kong, D., Zhang, L., 2022. Highly efficient metal-organic frameworks adsorbent for Pd (II) and Au (III) recovery from solutions: experiment and mechanism. Environ. Res. 210 (January), 112870 https://doi.org/10.1016/j.envres.2022.112870.

Teffu, D.M., Ramoroka, M.E., Makhafola, M.D., Makgopa, K., Maponya, T.C., Seerane, O. A., Hato, M.J., Iwuoha, E.I., Modibane, K.D., 2022. Electrochimica Acta High-performance supercabattery based on reduced graphene oxide / metal organic framework nanocomposite decorated with palladium nanoparticles. Electrochim. Acta 412 (March), 140136. https://doi.org/10.1016/j.electacta.2022.140136.

Uheida, A., Iglesias, M., Fontàs, C., Hidalgo, M., Salvadó, V., Zhang, Y.u., Muhammed, M., 2006. Sorption of palladium (II), rhodium (III), and platinum (IV) on Fe_3O_4 nanoparticles. J. Colloid Interface Sci. 301 (2), 402–408. https://doi.org/10.1016/j.jcis.2006.05.015.

Vo, T.K., Kim, W.S., Kim, J., 2020. Ethylenediamine-incorporated MIL-101(Cr)-NH_2 metal-organic frameworks for enhanced CO_2 adsorption. Korean J. Chem. Eng. 37 (7), 1206–1211. https://doi.org/10.1007/s11814-020-0548-8.

Wang, S., Vincent, T., Roux, J.C., Faurand, C., Guibal, E., 2017. Pd (II) and Pt (IV) sorption using alginate and algal-based beads. Chem. Eng. J. 313, 567–579. https://doi.org/10.1016/j.cej.2016.12.039.

Wang, L., Zhao, X., Zhang, J., Xiong, Z., 2017. Selective adsorption of Pb (II) over the zinc-based MOFs in aqueous solution-kinetics, isotherms, and the ion exchange mechanism. Environ. Sci. Pollut. Res. 24, 14198–14206. https://doi.org/10.1007/s11356-017-9002-9.

Wasikiewicz, J.M., Mitomo, H., Seko, N., Tamada, M., Yoshii, F., 2007. Platinum and palladium ions adsorption at the trace amounts by radiation crosslinked carboxymethylchitin and carboxymethylchitosan hydrogels. J. Appl. Polym. Sci. 104, 4015–4023. https://doi.org/10.1002/app.26034.

Yousif, A.M., 2019. Recovery and then individual separation of platinum, palladium, and rhodium from spent car catalytic converters using hydrometallurgical technique followed by successive precipitation methods. J. Chem. 2019, 7. https://doi.org/10.1155/2019/2318157.

Yuanpei, L., Wei, Z., Zhigang, T.A.I., Yaling, Y., Jun, S., Zonghao, L.I., 2012. Cloud point extraction and flame atomic absorption spectrometry analysis of palladium, platinum, and gold ions from industrial polluted soil. Rare Met. 31 (5), 512–516. https://doi.org/10.1007/s12598-012-0549-9.

Zhang, M., Lv, Y., Xu, Z., Wang, S., Wang, J., 2020. The removal of platinum group metals, Cs, Se, and Te from nuclear waste glass using liquid Sb extraction and phase separation methods. Mater. 13 (22), 5305. https://doi.org/10.3390/ma13225305.

Zhou, L., Liu, J., Liu, Z., 2009. Adsorption of platinum(IV) and palladium(II) from aqueous solution by thiourea-modified chitosan microspheres. J. Hazard. Mater. 172 (1), 439–446. https://doi.org/10.1016/j.jhazmat.2009.07.030.

Zhou, L., Xu, J., Liang, X., Liu, Z., 2010. Adsorption of platinum (IV) and palladium (II) from aqueous solution by magnetic cross-linking chitosan nanoparticles modified with ethylenediamine. J. Hazard. Mater. 182 (1–3), 518–524. https://doi.org/10.1016/j.jhazmat.2010.06.062.

Zhuo, N., Lan, Y., Yang, W., Yang, Z., Li, X., Zhou, X., Liu, Y., Shen, J., Zhang, X., 2017. Adsorption of three selected pharmaceuticals and personal care products (PPCPs) onto MIL-101(Cr)/natural polymer composite beads. Sep. Purif. Technol. 177, 272–280. https://doi.org/10.1016/j.seppur.2016.12.041.